

O₂ activation by binuclear Cu sites: Noncoupled versus exchange coupled reaction mechanisms

Peng Chen and Edward I. Solomon[†]

Department of Chemistry, Stanford University, Stanford, CA 94305

Edited by Jack Halpern, University of Chicago, Chicago, IL, and approved July 28, 2004 (received for review May 1, 2004)

Binuclear Cu proteins play vital roles in O₂ binding and activation in biology and can be classified into coupled and noncoupled binuclear sites based on the magnetic interaction between the two Cu centers. Coupled binuclear Cu proteins include hemocyanin, tyrosinase, and catechol oxidase. These proteins have two Cu centers strongly magnetically coupled through direct bridging ligands that provide a mechanism for the 2-electron reduction of O₂ to a $\mu\text{-}\eta^2\text{:}\eta^2$ side-on peroxide bridged Cu₂(O₂²⁻) species. This side-on bridged peroxo-Cu₂ species is activated for electrophilic attack on the phenolic ring of substrates. Noncoupled binuclear Cu proteins include peptidylglycine α -hydroxylating monooxygenase and dopamine β -monooxygenase. These proteins have binuclear Cu active sites that are distant, that exhibit no exchange interaction, and that activate O₂ at a single Cu center to generate a reactive Cu^{II}/O₂ species for H-atom abstraction from the C–H bond of substrates. O₂ intermediates in the coupled binuclear Cu enzymes can be trapped and studied spectroscopically. Possible intermediates in noncoupled binuclear Cu proteins can be defined through correlation to mononuclear Cu^{II}/O₂ model complexes. The different intermediates in these two classes of binuclear Cu proteins exhibit different reactivities that correlate with their different electronic structures and exchange coupling interactions between the binuclear Cu centers. These studies provide insight into the role of exchange coupling between the Cu centers in their reaction mechanisms.

Biological Cu centers play important roles in O₂ binding, activation, and reduction to H₂O (1). Hemocyanin (Hc), tyrosinase (Tyr), and catechol oxidase (CO) are well studied systems and contain similar binuclear Cu active sites in which the two Cu centers are close in distance (≈ 3.6 Å) with strong magnetic interactions (1, 2). The binuclear Cu center in Hc reversibly binds O₂, whereas the binuclear Cu active sites in Tyr and CO activate O₂ for substrate hydroxylation/oxidation. Upon O₂ binding, these binuclear Cu proteins generate the same Cu₂^{II}(O₂²⁻) peroxide intermediate, where the O₂²⁻ binds in a $\mu\text{-}\eta^2\text{:}\eta^2$ side-on bridging fashion providing a direct orbital overlap pathway for the 2-electron (e⁻) reduction of O₂ to peroxide (3). This side-on Cu₂^{II}(O₂²⁻) species has been extensively characterized, both in model systems and trapped protein intermediates, and exhibits characteristic spectral features, including an intense charge transfer (CT) transition at ≈ 350 nm ($\epsilon \approx 20,000$ M⁻¹·cm⁻¹) in its absorption spectrum and a very low $\nu_{\text{O-O}}$ vibrational frequency (≈ 750 cm⁻¹) in its resonance Raman (rR) spectrum (1, 2). These spectral features result from the side-on bound peroxide π_{σ}^* orbital charge donation and the σ^* backbonding interactions with the Cu^{II} $d_{x^2-y^2}$ orbitals [Fig. 1A, π_{σ}^* donor, lowest unoccupied molecular orbital (LUMO), and B, σ^* acceptor, highest occupied molecular orbital (HOMO)]. These Cu₂^{II}-peroxide bonding interactions lead to a large energy splitting between the LUMO and HOMO of the side-on Cu₂^{II}(O₂²⁻) species and the strong antiferromagnetic coupling between its two Cu^{II} centers. In Tyr, the large peroxide

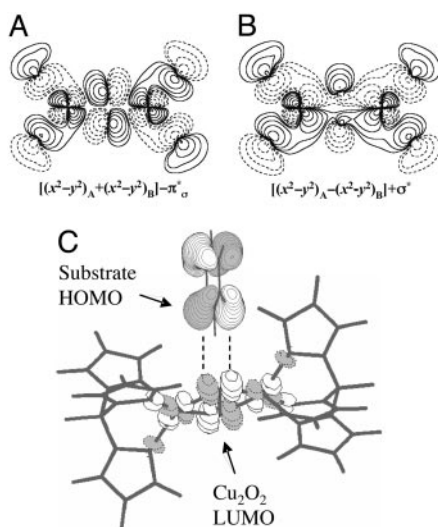


Fig. 1. FMO of the side-on Cu₂(O₂²⁻) species. (A and B) Contour plots of the LUMO (A) and HOMO (B) of the side-on Cu₂(O₂²⁻) species showing peroxide π_{σ}^* donation and σ^* backbonding interactions with the Cu^{II} $d_{x^2-y^2}$ orbitals. (C) Frontier molecular orbitals of the phenyl HOMO and side-on Cu₂(O₂²⁻) LUMO showing the orbital overlap for electrophilic attack.

π_{σ}^* to Cu charge donation results in significant peroxide character in the LUMO (Fig. 1A), which activates the side-on Cu₂(O₂²⁻) species for electrophilic attack at the phenolic ring of the substrate, leading to its hydroxylation (Fig. 1C). The σ^* backbonding interaction (in Fig. 1B) weakens the O–O bond, facilitating its cleavage.

Based on the strong magnetic exchange interaction between the Cu centers [quantitated by the exchange coupling constant J ($H = -2JS_1S_2$)], Hc, Tyr, and CO have been classified as coupled binuclear Cu proteins (1). In contrast, noncoupled binu-

clear Cu proteins have two structurally inequivalent Cu centers largely separated in space (≈ 11 Å) with no direct bridging ligand and no observable magnetic interaction (4–6). This class of binuclear Cu proteins includes peptidylglycine α -hydroxylating monooxygenase (PHM) and dopamine β -monooxygenase (D β M), both of which catalyze substrate C–H bond hydroxylation (a Gly backbone C–H bond in PHM or a dopamine benzylic C–H bond in D β M) in a stereo- and regiospecific fashion by means of an H-atom abstraction mechanism (4). This C–H bond H-atom abstraction is performed by a reactive mononuclear Cu^{II}/O₂ species at the Cu_M site [alternatively labeled Cu_B (6)]. The other Cu_H site [alternatively labeled Cu_A (6)] provides an additional electron through long-range electron transfer (ET) to the Cu_M site. Because the two Cu centers in PHM and D β M showed no electronic coupling (i.e., noncoupled), the mechanism for this intramolecular long-range ET was not clear. A superoxide-channeling mechanism (7) and a substrate-facilitated ET mechanism (8, 9) were proposed to account for this inter-Cu ET process.

In contrast to the well studied side-on Cu₂(O₂²⁻) species in coupled binuclear proteins, the nature of the reactive mononuclear Cu^{II}/O₂ species in PHM and D β M was unclear. Structural information from crystallographic (6, 8) and EXAFS (extended x-ray absorption fine structure) studies (10–12), combined with recent advances in spectroscopic

This paper was submitted directly (Track II) to the PNAS office.

[†]To whom correspondence should be addressed. E-mail: edward.solomon@stanford.edu.

© 2004 by The National Academy of Sciences of the USA

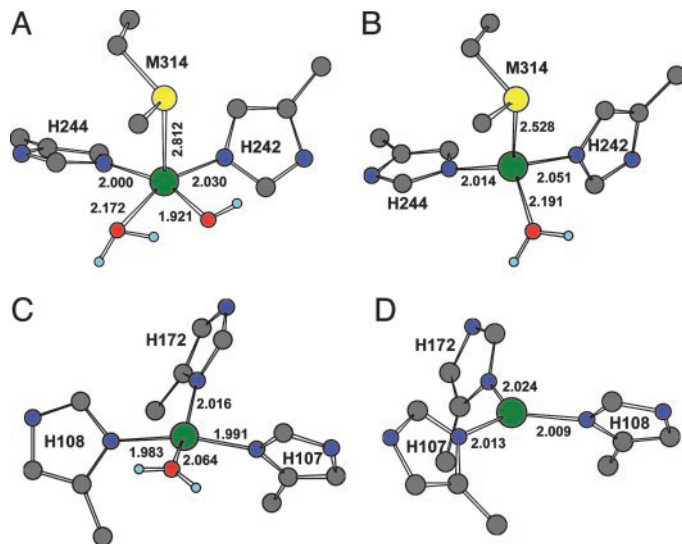


Fig. 2. Geometry-optimized structures of resting oxidized (A) and reduced (B) Cu_M site and resting oxidized (C) and reduced (D) Cu_H site.

characterization coupled with density functional theory (DFT) calculations, have defined geometric and electronic structural models of the resting oxidized and reduced Cu_M and Cu_H sites (Fig. 2) (13). In correlation to detailed spectroscopic and electronic structure studies of related model complexes (14, 15), DFT calculations have been used to evaluate two possible mononuclear $\text{Cu}^{\text{II}}/\text{O}_2$ species proposed to be the intermediates in the H-atom abstraction reactivity in PHM and $\text{D}\beta\text{M}$ (16): a 2-e^- reduced $\text{Cu}_M^{\text{II}}\text{-OOH}$ species and an 1-e^- reduced $\text{Cu}_M^{\text{II}}\text{-superoxide}$ species. These studies generated a reasonable reaction coordinate for the H-atom abstraction reaction in PHM and $\text{D}\beta\text{M}$, involving the mononuclear $\text{Cu}_M^{\text{II}}\text{-superoxide}$ species. The $\text{Cu}_M^{\text{II}}\text{-superoxide}$ intermediate is consistent with and further supported by recent kinetic studies on $\text{D}\beta\text{M}$ (17). These studies on the non-coupled binuclear Cu enzymes PHM and $\text{D}\beta\text{M}$ reveal a very different reaction mechanism from that of the coupled binuclear Cu proteins and define important contributions from the differences in exchange coupling to variation in O_2 activation by binuclear Cu enzymes.

Electronic Structure Descriptions of Possible Mononuclear $\text{Cu}_M^{\text{II}}/\text{O}_2$ Intermediates: Frontier Molecular Orbitals (FMOs) for H-atom Abstraction

Spectroscopic studies combined with DFT calculations can provide detailed electronic structure descriptions of $\text{Cu}_n\text{-O}_2$ species (1). Electronic structure descriptions provide insight into relative chemical reactivities (18), for which the energies, molecular orbital coefficients,

and overlaps of FMOs (i.e., low-energy unoccupied and high-energy occupied molecular orbitals, particularly the LUMO and HOMO) play important roles in activating specific reaction coordinates and can be obtained from DFT calculations (1). In this section, we describe the acceptor FMOs of the $\text{Cu}_M^{\text{II}}\text{-OOH}$ and $\text{Cu}_M^{\text{II}}\text{-superoxide}$ species at the Cu_M site in PHM, extended from spectroscopic results on well defined model complexes and consider their relative activation for H-atom abstraction.

The $\text{Cu}_M^{\text{II}}\text{-OOH}$ Intermediate. The spectroscopically calibrated and DFT optimized structure of the putative $\text{Cu}_M^{\text{II}}\text{-OOH}$ intermediate has a square pyramidal geometry with the OOH^- bound in an end-on fashion (Fig. 3A) (13). The lowest energy acceptor orbital of $\text{Cu}_M^{\text{II}}\text{-OOH}$ for H-atom abstraction is the spin-down LUMO, which is a Cu d -based orbital ($\approx 61\%$ Cu character) with low $\text{OOH}^- \pi_\sigma^*$ character ($\approx 19\%$) because of a Cu- OOH pseudo- σ bonding interaction that is not very covalent (Fig. 3B). The $\text{OOH}^- \pi_\sigma^*$ component of this spin-down LUMO is highly polarized toward the Cu with a limited coefficient (2%) on the remote oxygen atom, indicating that the spin-down LUMO is, in fact, not a good acceptor orbital for H-atom abstraction. Another possible H-atom abstraction acceptor orbital, the $\text{OOH}^- \sigma^*$ orbital, is ≈ 3 eV ($1 \text{ eV} = 1.602 \times 10^{-19} \text{ J}$) higher in energy than the spin-down LUMO and has a large coefficient on the O_2 moiety (53%, Fig. 3C). However, the σ^* orbital is similarly polarized toward the Cu, resulting in a much lower molecular orbital coefficient on the remote oxygen

atom (13%). This polarization is mainly due to the effect of protonation and is generally observed for Cu^{II} bound OOH^- (13, 14, 19), giving rise to a strengthened O-O bond.

This increased O-O bond strength is best probed experimentally by rR spectroscopy, where the $\nu_{\text{O-O}}$ frequency and its ^{18}O isotope shift can be used (along with the Cu-O modes) to determine the O-O force constant $k_{\text{O-O}}$ by means of a normal coordinate analysis. Fig. 3D gives the rR spectra of a related mononuclear model complex, $\text{L3Cu}^{\text{II}}\text{-OOH}$ [where L3 is hydrotris(3-*tert*-butyl-5-isopropyl-1-pyrazolyl)borate] (14). The $\nu_{\text{O-O}}$ vibration of $\text{L3Cu}^{\text{II}}\text{-OOH}$ occurs at 843 cm^{-1} and shifts to 799 cm^{-1} upon ^{18}O labeling. These rR data give a $k_{\text{O-O}}$ for $\text{L3Cu}^{\text{II}}\text{-OOH}$ of 3.51 mdyne/\AA ($1 \text{ dyne} = 10 \mu\text{N}$), which is higher than those of unprotonated $\text{Cu}^{\text{II}}\text{-O}_2^-$ species (Table 1, row E), reflecting the strengthened O-O bond from protonation-induced polarization. The facts that the σ^* orbital has a low coefficient on the remote oxygen atom because of polarization and is high in energy indicate that it is also an ineffective pathway for H-atom abstraction. Therefore, the electronic structure description of the putative $\text{Cu}_M^{\text{II}}\text{-OOH}$ intermediate suggested that it has a strong O-O bond that is not significantly activated for H-atom abstraction.

The Side-On $\text{Cu}_M^{\text{II}}\text{-Superoxide}$ Intermediate.

The optimized lowest energy structure of the $\text{Cu}_M^{\text{II}}\text{-superoxide}$ intermediate has the superoxide ligand bound equatorially in a side-on fashion, forming a square pyramidal geometry around the Cu center with a Met as the long axial ligand (Fig. 4A) (16). This side-on geometry is very similar to the crystal structure of a well characterized side-on $\text{Cu}^{\text{II}}\text{-superoxide}$ model complex $\text{LCu}^{\text{II}}\text{O}_2^-$ (where L is the trispyrazolylborate ligand). The superoxide nature of this complex was experimentally determined from its $\nu_{\text{O-O}}$ frequency ($1,043 \text{ cm}^{-1}$) and ^{18}O isotope shift ($\Delta\nu = 59 \text{ cm}^{-1}$) (Fig. 4D) (15, 20). The lowest energy acceptor orbital of the $\text{Cu}_M^{\text{II}}\text{-superoxide}$ intermediate (i.e., the FMO for H-atom abstraction) is its LUMO, which is the antibonding combination of the Cu $d_{x^2-y^2}$ and superoxide π_σ^* orbitals (Fig. 4B) (16). The Cu $d_{x^2-y^2}$ and superoxide π_σ^* orbitals are in the CuO_2 plane and have a large σ -type orbital overlap, resulting in a highly covalent singlet ground state with a large O_2^- coefficient (64%, Fig. 4B). This highly covalent $\text{Cu}^{\text{II}}\text{-superoxide}$ interaction contributes to the formation of this complex as the 1-e^- reduction of O_2 is energetically less favorable than the 2-e^- process (see below).

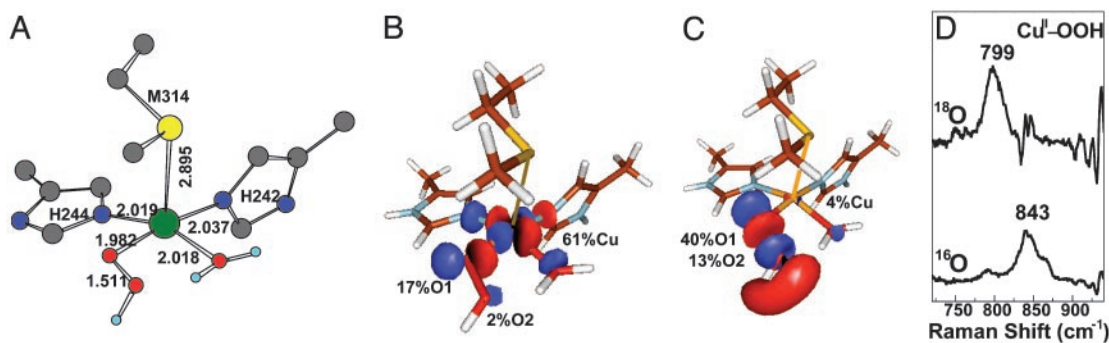


Fig. 3. Acceptor FMOs of the $\text{Cu}^{\text{II}}\text{-OOH}$ intermediate. (A) Geometry-optimized structure of $\text{Cu}^{\text{II}}\text{-OOH}$. (B) Spin-down LUMO (x^2-y^2)- π^* . (C) Peroxide σ^* orbital. (D) rR spectra of the $\text{Cu}^{\text{II}}\text{-OOH}$ model complex in the $\nu_{\text{O-O}}$ region excited at 568.2 nm (14).

The Cu^{II} center ($S = 1/2$) and the superoxide ligand ($S = 1/2$) can, in principle, have either a singlet or a triplet ground state for the $\text{Cu}^{\text{II}}\text{-superoxo}$ intermediate. The diamagnetic singlet ground state of the $\text{Cu}^{\text{II}}\text{-superoxo}$ intermediate was confirmed experimentally by SQUID (superconducting quantum interfering device) magnetic susceptibility measurements for the $\text{Cu}^{\text{II}}\text{-superoxo}$ model complex (Fig. 4E), which showed that the effective magnetic moment (μ_{eff}) is close to zero at low temperature, as compared with $\mu_{\text{eff}} \approx 2.83$ Bohr magnetons for a triplet state (15). Additionally, the μ_{eff} deviates from zero at higher temperatures (Fig. 4E) because of the thermal population of an excited triplet state at $\approx 1,500 \text{ cm}^{-1}$. This triplet state is in fact not related to the singlet ground state, which involves a spin pair in the $d_{x^2-y^2}/\pi^*$ orbital in the Cu-O_2 plane. This low-lying triplet derives from

the interaction between the Cu^{II} $d_{x^2-y^2}$ and the superoxide π^* orbitals (Fig. 4C Upper Right). The corresponding π^* singlet state ${}^1\Gamma(\pi^*)$ is higher in energy than the triplet state because of the orthogonality of the two interacting orbitals and was observed experimentally as a low energy weak CT transition at $\approx 4,200 \text{ cm}^{-1}$ in the absorption spectrum of $\text{LCu}^{\text{II}}\text{O}_2$ (Fig. 4F) (15). The triplet state associated with the ground state singlet involves excitation of an electron from the $\pi^* + d_{x^2-y^2}$ to the $d_{x^2-y^2} - \pi^*$ orbital, ${}^3\Gamma(\pi^*)$, and its corresponding singlet ${}^1\Gamma(\pi^*)$ can be reached by means of an allowed CT transition. This CT transition should be intense in the absorption spectrum because of the large overlap between the superoxide π^* and Cu $d_{x^2-y^2}$ orbitals (Fig. 4C). Experimentally, no intense CT transition was observed at energies up to $\approx 30,000 \text{ cm}^{-1}$, indicating a large splitting of the bond-

ing and antibonding combinations of the Cu $d_{x^2-y^2}$ and superoxide π^* orbitals resulting from their highly covalent interaction (Fig. 4B and C). This strong interaction leads to a covalently delocalized singlet ground state for the side-on $\text{Cu}^{\text{II}}\text{-superoxo}$ species with no spin polarization (i.e., no net antiparallel spin localization on the Cu^{II} and the superoxide ligand), arguing against an antiferromagnetic exchange-coupled description (or biradical) previously used for the diamagnetism of $\text{Cu}^{\text{II}}\text{-superoxo}$ species (21–23).

The electronic structure description of the covalently delocalized singlet ground state of the $\text{Cu}^{\text{II}}\text{-superoxo}$ intermediate provides insight into its possible reactivity in H-atom abstraction. The LUMO of the $\text{Cu}^{\text{II}}\text{-superoxo}$ intermediate is low in energy relative to the spin-down LUMO and the σ^* orbital of the $\text{Cu}^{\text{II}}\text{-OOH}$ intermediate ($\approx 4.4 \text{ eV}$ lower than the $\text{Cu}^{\text{II}}\text{-OOH}$ σ^* orbital) and has a large orbital coefficient on the O_2^- moiety (Fig. 4B versus Fig. 3B and C). Therefore, a $\text{Cu}^{\text{II}}\text{-superoxo}$ intermediate should be much more effective in H-atom abstraction than the putative $\text{Cu}^{\text{II}}\text{-OOH}$ intermediate in PHM chemistry. These FMO differences should lead to differences in thermodynamics and kinetic barriers as discussed below.

Correlation of Electronic Structure to Reactivity

The electronic structures derived from model studies coupled with the FMO analysis presented above provided initial insight into the relative H-atom abstraction reactivities of the $\text{Cu}^{\text{II}}\text{-OOH}$ and $\text{Cu}^{\text{II}}\text{-superoxo}$ intermediates. In this section, we quantitatively compare the energetics and energy barriers of these two $\text{Cu}^{\text{II}}\text{-O}_2$ species calculated along the reaction coordinate of H-atom abstraction.

$\text{Cu}^{\text{II}}\text{-OOH}$ Reaction Coordinate. As predicted from the above electronic

Table 1. Summary of $\nu_{\text{O-O}}$ frequencies and $k_{\text{O-O}}$ force constants of binuclear and mononuclear Cu-O_2 species

	Nature of ligand	Structure	$\nu_{\text{O-O}}$, cm^{-1}	$k_{\text{O-O}}$, $\text{mdyne}/\text{\AA}$
A	Peroxo		763	2.43
B	Peroxo		832	3.17
C	Hydroperoxo		880	3.52
D	Peroxo		803	2.90
E	Hydroperoxo		843	3.51
F	Peroxo		968	—
G	Oxo		NA	NA
H	Superoxo		1,043	5.72

N/A, not applicable. —, not determined. See refs. 14, 15, 19, 35, and 37–39.

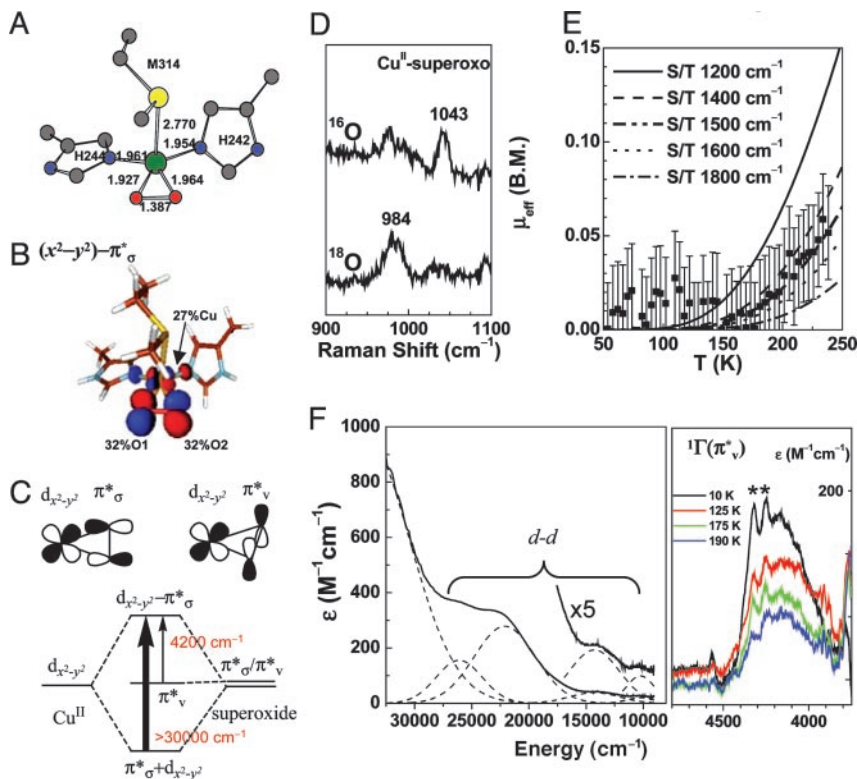
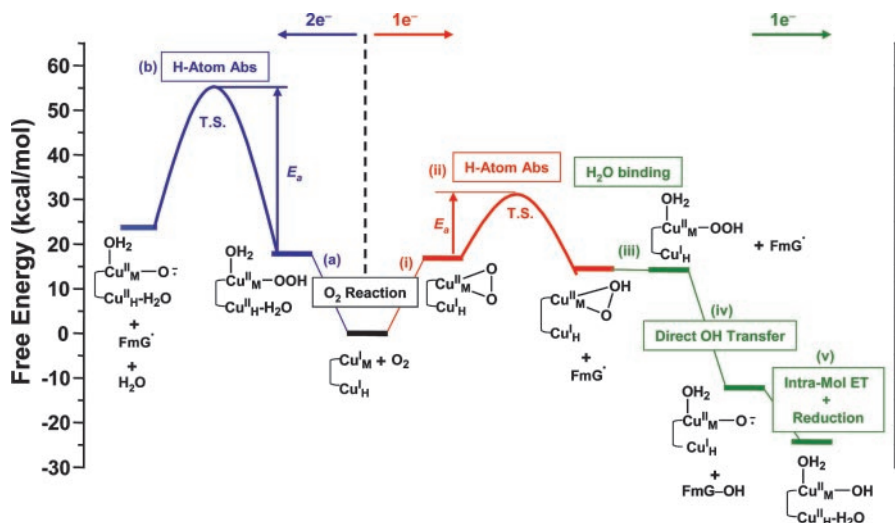


Fig. 4. Electronic structure and spectroscopy of the Cu^{II} -superoxo species. (A) Geometry-optimized structure of Cu^{II} -superoxo. (B) Acceptor FMO (LUMO) of Cu^{II} -superoxo. (C) Schematic diagram of the interaction between the Cu^{II} $d_{x^2-y^2}$ and superoxide π^*_σ/π^*_ν orbitals. The arrows and their widths indicate the expected CT transitions (singlets) and their relative intensities. (D) rR spectra in the $\nu_{\text{O-O}}$ region. (E) SQUID magnetic susceptibility measured effective magnetic moment μ_{eff} . B.M., Bohr magneton. Lines are the simulated curves assuming different singlet/triplet energy splittings, $S/T = E_5 = 1 - E_5 = 0$. (F) Absorption spectra of the Cu^{II} -superoxo model complex. (Left) UV/visible Cu^{II} $d-d$ transitions assigned. (Right) Near-infrared CT. Vibrational overtones of mulling agent are labeled by asterisks (15).

structure description, the $\text{Cu}^{\text{II}}_M\text{-OOH}$ species does not appear to be activated for H-atom abstraction. The calculated potential energy surface along the H-atom transfer coordinate for the $\text{Cu}^{\text{II}}_M\text{-OOH}$ intermediate is shown in blue in Scheme 1, step b, by using a small substrate analogue formylglycine (FmG) (16). This reaction generates the substrate radical FmG^\cdot , a H_2O product, and a $\text{Cu}^{\text{II}}_M\text{-oxyl}$ species. In contrast to the $\text{L3Cu}^{\text{II}}\text{OOH}$ model complex, the ΔG of this reaction is thermodynamically accessible [$\approx 6\text{--}7$ kcal/mol (1 cal = 4.18 J)]. This small ΔG is due to the energy difference (≈ 22 kcal/mol) between the strong O-H bond of the H_2O product and the activated C-H bond of the FmG reactant from resonance delocalization of the FmG^\cdot radical generated, combined with stabilization by the Met ligand, which binds in an equatorial position in the $\text{Cu}^{\text{II}}_M\text{-oxyl}$ species in contrast to its axial coordination in $\text{Cu}^{\text{II}}_M\text{-OOH}$ in Fig. 3A (16). However, consistent with the FMO analysis of $\text{Cu}^{\text{II}}_M\text{-OOH}$, the potential energy surface along the H-atom transfer reaction coordinate

showed a large energy barrier of ≈ 37 kcal/mol, making this reaction kinetically highly unlikely. Therefore,



Scheme 1. Summary of the 2-e^- (left) and 1-e^- (right) reaction pathways in PHM (16). For clarity, His and Met ligands are omitted in the structures. Only species that are essential to the reactions are indicated on the scheme. Free energies are referenced to the initial reactions, which are set to zero. The proton and H_2O ligand in steps v and a and the H_2O ligand in step iii are from the solvent. T.S., transition state.

H-atom abstraction by the $\text{Cu}^{\text{II}}_M\text{-OOH}$ intermediate is an energetically plausible but kinetically unfavorable reaction pathway in PHM (16).

$\text{Cu}^{\text{II}}_M\text{-Superoxo}$ Reaction Coordinate. In contrast to the $\text{Cu}^{\text{II}}_M\text{-OOH}$ species, the calculated energetics and energy barrier indicated that $\text{Cu}^{\text{II}}_M\text{-superoxo}$ is very reactive in H-atom abstraction, as predicted from the above electronic structure description. The calculated potential energy surface for the $\text{Cu}^{\text{II}}_M\text{-superoxo}$ intermediate H-atom abstraction reaction is shown in red in Scheme 1, step ii. This reaction generates the substrate radical FmG^\cdot and an asymmetrically side-on bound $\text{Cu}^{\text{II}}_M\text{-hydroperoxo}$ species that can readily convert to the end-on bound $\text{Cu}^{\text{II}}_M\text{-OOH}$ intermediate (Fig. 3A) by binding an H_2O molecule ($\Delta G \approx -0.3$ kcal/mol) (16). The energetics of this H-atom abstraction reaction is almost thermo-neutral, ≈ 2 kcal/mol. More importantly, because of its highly covalent FMO, the energy barrier along the H-atom transfer coordinate is only ≈ 14 kcal/mol (Scheme 1, step ii), which is much lower than that for the $\text{Cu}^{\text{II}}_M\text{-OOH}$ intermediate (≈ 37 kcal/mol) at the same active site/substrate distance (Scheme 1, step b). Therefore, the favorable reaction energetics and the low energy barrier indicate that the $\text{Cu}^{\text{II}}_M\text{-superoxo}$ H-atom abstraction reaction is a highly favorable pathway in PHM both thermodynamically and kinetically.

A reasonable reaction pathway for completion of the substrate hydroxylation was determined in ref. 16 and is summarized in Scheme 1 (green steps). After the H-atom abstraction reaction, the $\text{Cu}^{\text{II}}_M\text{-OOH}$ intermediate and the

FmG• radical generated can undergo a direct OH group transfer to form the hydroxylated product FmG-OH and a Cu_M^{II}-oxyl species, driven by the formation of a strong product C–O bond (Scheme 1, step iv) (16). (An alternative reaction pathway, in which the Cu_M^{II}-OOH species undergoes reductive O–O bond cleavage by means of ET from Cu_H coupled to protonation, is ≈20 kcal/mol uphill in Δ*G* because of the unfavorable 1-e[−] reduction of the peroxide.) The Cu_M^{II}-oxyl species produced can then be reduced to the stable resting Cu_M^{II} site by the Cu_H^I site by an intramolecular ET process and protonation from solvent (Scheme 1, step v). This long-range ET-coupled reduction process is downhill in free energy (Δ*G* ≈ −12 kcal/mol), which is due to the relatively high-energy nature of the Cu_M^{II}-oxyl species that provides the necessary driving force to complete the reaction.

With an additional H₂O ligand at the Cu_M site, geometry optimization gave an end-on Cu^{II}-superoxo species (Scheme 1, step i), which is ≈11 kcal/mol higher in free energy than the side-on Cu_M^{II}-superoxo intermediate (16). The LUMO of the end-on Cu^{II}-superoxide species is also an antibonding combination of Cu *d*_{x²−y²} and superoxide π*_σ orbitals with similar molecular orbital coefficients on the oxygen atoms to those of the side-on Cu_M^{II}-superoxo intermediate. Based on its electronic structure description and FMO theory, this end-on superoxide species is predicted to be comparable to or slightly less reactive than the side-on superoxide species, not considering the steric effects of their different binding geometries (16). The structure of a Cu–O₂ intermediate in PHM has recently been solved and has a four-coordinate Cu with O₂ binding in an end-on mode (24). The nature of the Cu–O₂ species in the structure is not known (i.e., Cu^I-O₂, Cu^{II}-superoxide, Cu^{II}-peroxide, Cu^{II}-OOH, etc.), and further spectroscopic studies are needed to define this intermediate. In light of the reaction mechanism presented here for PHM and DβM, it might correspond to the end-on Cu^{II}-superoxide species geometry-optimized with an additional H₂O ligand (without the H₂O, it optimizes to the side-on structure) or the Cu_M^{II}-OOH species generated by the H-atom abstraction (Scheme 1, step iii), both of which have a similar end-on Cu–O–O geometry. However, the O–O bond length of the Cu–O₂ intermediate in the crystal structure may be too short for a peroxo species (24).

Structure/Function Correlations: Noncoupled Versus Exchange-Coupled Binuclear Cu Sites

Electronic structure descriptions combined with FMO analyses and reaction coordinate calculations indicate that the 1-e[−] reduced Cu_M^{II}-superoxo species is likely the reactive Cu^{II}/O₂ species in H-atom abstraction by PHM, as compared with the 2-e[−] reduced Cu_M^{II}-OOH species. This Cu_M^{II}-superoxo mechanism is consistent with the kinetic studies by Evans *et al.* (17). The reaction pathway summarized in Scheme 1 (steps in red and green), from the formation of the Cu_M^{II}-superoxo intermediate to the H-atom abstraction reaction, and the completion of the substrate hydroxylation also provide insight into the mechanism of the inter-Cu intramolecular ET process involved in the PHM/DβM reaction and the role of the nonmagnetically coupled nature of their active sites, as compared with the coupled binuclear Cu proteins.

The direct bridging of the two Cu centers in the binuclear Cu proteins Hc, Tyr, and CO provides a mechanism for O₂ reduction by two electrons to the side-on Cu₂^{II}(O₂^{2−}) species (3) and results in the strong Cu–Cu antiferromagnetic exchange coupling (−2*J* ≥ 1,200 cm^{−1}) (25). This side-on Cu₂^{II}(O₂^{2−}) peroxo species is activated for electrophilic attack at the phenyl ring of substrates (Fig. 1C). In contrast, there is no observable magnetic interaction (i.e., very small *J*) between the two Cu centers in the noncoupled binuclear Cu protein PHM and DβM (26), because of the large Cu–Cu distance (≈11 Å in PHM) (6, 8). Thus, a long-range intramolecular ET process is required at some stage in the mechanism for the enzymatic reactions in PHM and DβM. Marcus theory governs the ET rate constant *k*_{ET} (27):

$$k_{ET} = \sqrt{\frac{\pi}{(h/2\pi)^2 \lambda k_B T}} (H_{DA})^2 \exp\left[-\frac{(\Delta G + \lambda)^2}{4\lambda k_B T}\right]$$

where *H*_{DA} is the donor/acceptor electronic coupling matrix element, Δ*G* is the driving force, and λ is the reorganization energy, which includes the active site geometry change (λ_{inner}) and the reorientation of the solvent dipoles (λ_{outer}, λ = λ_{inner} + λ_{outer}) associated with redox. The electronic coupling matrix element *H*_{DA} is related to the exchange constant *J*:

$$-2J = \frac{(H_{DA})^2}{U}$$

where *U* is the metal–metal CT energy (25, 28). Because *J* is small for the noncoupled Cu_M and Cu_H sites, the (*H*_{DA})² between the two Cu centers also must be small. Significant geometry changes between the reduced and oxidized forms of the Cu_M and Cu_H sites have been observed experimentally (10–12, 29) and are also found in calculated structures (13, 16), which suggest a large reorganization energy (λ_{inner}) is also associated with their redox reactions (Fig. 2, A, B, C, and D, respectively). [Note that the crystal structures of PHM (6, 8) did not resolve significant differences between the oxidized and the reduced proteins, whereas EXAFS results showed significant geometry changes upon redox (10–12). EXAFS studies are more accurate in determining the metal–ligand bond lengths and differentiating Cu oxidation states.] Therefore, to have a significant *k*_{ET}, there must be a large driving force Δ*G* for the ET process from Cu_H to Cu_M. The reaction mechanism in Scheme 1 indicates that PHM could achieve this driving force through a direct OH transfer to the substrate FmG• radical after the H-atom abstraction step (Scheme 1, step iv). The reduction and protonation of the high-energy Cu_M^{II}-oxyl species formed could provide the necessary driving force for the intramolecular ET from the Cu_H^I site (Scheme 1, step v). This thermodynamically driven ET mechanism also suggests that superoxide channeling (7) is not a necessary event for the ET process; furthermore, neither is the substrate-mediated ET mechanism (8), because no change was observed in the EPR spectrum of resting PHM upon substrate binding, which indicates that the *J* value between the two Cu centers is still very small when the substrate is present (13).

The noncoupled nature of the PHM/DβM active sites is strongly correlated with their chemistry. If two Cu centers are strongly exchange-coupled, the O₂ reaction with the reduced protein would lead to fast ET from both Cu sites to O₂, generating a 2-e[−] reduced binuclear- or mononuclear-Cu^{II}-peroxide level species (O₂^{2−}), depending on the distance between the two Cu atoms (Table 1, rows A–E). These Cu^{II}-peroxo/hydroperoxo complexes do not appear to be reactive in H-atom abstraction (1, 5, 30–34), nor is the mononuclear Cu_M^{II}-OOH species considered above (13, 16). Although 4-e[−] reduction of O₂ by two Cu atoms could lead to a bis-μ-oxo-Cu₂^{III} species (Table 1, row G), which is very reactive in H-atom abstraction, the existence of the Cu^{III} oxidation state in a biological environment is not known and likely not accessible because of the inability of biological ligands (His, etc.) to stabilize the Cu^{III} oxidation state.

The inaccessible oxidation state is also the case for the mononuclear Cu^{III}-peroxide species (Table 1, row F), which was recently synthesized with an exceptionally strong electron-donating ligand (35). Therefore, to form the 1-e⁻ reduced superoxide level species Cu_M^{II}-superoxo, which from the above model would be the reactive species in H-atom abstraction and not proceed further to a thermodynamically favored 2-e⁻ reduced peroxo species [at pH = 7, E°(O₂/H₂O₂) = 0.28 V, E°(O₂/O₂⁻) = -0.33 V versus normal hydrogen electrode] (36), the two Cu sites have to be nonelectronically coupled. This noncoupled nature of the binuclear Cu

active site provides a strategy for PHM and DβM to form a reactive Cu^{II}-superoxo species at one Cu site (Cu_M) for the required H-atom abstraction reactivity while maintaining the ability to provide an additional electron from another Cu site (Cu_H) to complete the reaction, the intramolecular ET being switched on by a high driving force at the appropriate step in the enzymatic reaction cycle.

In summary, the mononuclear reactive Cu^{II}/O₂ species in the noncoupled binuclear Cu proteins gives a different reaction mechanism in O₂ activation and substrate hydroxylation from that of the coupled binuclear Cu proteins. The ex-

tent of magnetic exchange coupling between the two Cu centers in these two classes of binuclear Cu proteins plays an important role in determining the formation of the reactive Cu_n^{II}-O₂ species and thus their resulting reactivities (H-atom abstraction versus electrophilic attack).

We thank Drs. Betty Eipper and Joseph Bell for collaboration. The research was supported by National Institutes of Health Grant DK-31450 (to E.I.S.). P.C. was supported by a Gerhard Casper Stanford Graduate Fellowship and a Franklin Veatch Memorial Fellowship.

- Solomon, E. I., Chen, P., Metz, M., Lee, S.-K. & Palmer, A. E. (2001) *Angew. Chem. Int. Ed.* **40**, 4570–4590.
- Solomon, E. I., Sundaram, U. M. & Machonkin, T. E. (1996) *Chem. Rev.* **96**, 2563–2606.
- Metz, M. & Solomon, E. I. (2001) *J. Am. Chem. Soc.* **123**, 4938–4950.
- Klinman, J. P. (1996) *Chem. Rev.* **96**, 2541–2562.
- Liang, H.-C., Dahan, M. & Karlin, K. D. (1999) *Curr. Opin. Chem. Biol.* **3**, 168–175.
- Prigge, S. T., Kolhekar, A. S., Eipper, B. A., Mains, R. E. & Amzel, L. M. (1997) *Science* **278**, 1300–1305.
- Jaron, S. & Blackburn, N. J. (1999) *Biochemistry* **38**, 15086–15096.
- Prigge, S. T., Kolhekar, A. S., Eipper, B. A., Mains, R. E. & Amzel, L. M. (1999) *Nat. Struct. Biol.* **6**, 976–983.
- Bell, J., Meskini, R. E., D'Amato, D., Mains, R. E. & Eipper, B. A. (2003) *Biochemistry* **42**, 7133–7142.
- Blackburn, N. J., Rhames, F. C., Ralle, M. & Jaron, S. (2000) *J. Biol. Inorg. Chem.* **5**, 341–353.
- Boswell, J. S., Reedy, B. J., Kulathila, R., Merkler, D. J. & Blackburn, N. J. (1996) *Biochemistry* **35**, 12241–12250.
- Blackburn, N. J., Hasnain, S. S., Pettingill, T. M. & Strange, R. W. (1991) *J. Biol. Chem.* **266**, 23120–23127.
- Chen, P., Bell, J., Eipper, B. A. & Solomon, E. I. (2004) *Biochemistry* **43**, 5735–5747.
- Chen, P., Fujisawa, K. & Solomon, E. I. (2000) *J. Am. Chem. Soc.* **122**, 10177–10193.
- Chen, P., Root, D. E., Campochiaro, C., Fujisawa, K. & Solomon, E. I. (2003) *J. Am. Chem. Soc.* **125**, 466–474.
- Chen, P. & Solomon, E. I. (2004) *J. Am. Chem. Soc.* **126**, 4991–5000.
- Evans, J. P., Ahn, K. & Klinman, J. P. (2003) *J. Biol. Chem.* **278**, 49691–49698.
- Fleming, I. (1976) *Frontier Orbitals and Organic Chemical Reactions* (Wiley, New York).
- Root, D. E., Mahroof-Tahir, M., Karlin, K. D. & Solomon, E. I. (1998) *Inorg. Chem.* **37**, 4838–4848.
- Fujisawa, K., Tanaka, M., Moro-oka, Y. & Kitajima, N. (1994) *J. Am. Chem. Soc.* **116**, 12079–12080.
- Nappa, M., Valentine, J. S., Miksztal, A. R., Schugar, H. J. & Isied, S. S. (1979) *J. Am. Chem. Soc.* **101**, 7744–7746.
- Chaudhuri, P., Hess, M., Weyhermuller, T. & Wieghardt, K. (1999) *Angew. Chem. Int. Ed.* **38**, 1095–1098.
- Cramer, C. J., Tolman, W. B., Theopold, K. H. & Rheingold, A. L. (2003) *Proc. Natl. Acad. Sci. USA* **100**, 3635–3640.
- Prigge, S. T., Eipper, B. A., Mains, R. E. & Amzel, L. M. (2004) *Science* **304**, 864–867.
- Tuczek, F. & Solomon, E. I. (2001) *Coord. Chem. Rev.* **219–221**, 1075–1112.
- Ljones, T. & Skotland, T. (1984) in *Copper Proteins and Copper Enzymes*, ed. Lontie, R. (CRC Press, Boca Raton, FL), pp. 131–157.
- Marcus, R. A. & Sutin, N. (1985) *Biochim. Biophys. Acta* **811**, 265–322.
- Brunold, T. C., Gamelin, D. R. & Solomon, E. I. (2000) *J. Am. Chem. Soc.* **122**, 8511–8523.
- Scott, R. A., Sullivan, R. J., DeWolf, W. E., Jr., Dolle, R. E. & Kruse, L. I. (1988) *Biochemistry* **27**, 5411–5417.
- Kitajima, N. & Moro-oka, Y. (1994) *Chem. Rev.* **94**, 737–757.
- Decker, H., Dillinger, R. & Tuczek, F. (2000) *Angew. Chem. Int. Ed.* **39**, 1591–1595.
- Schindler, S. (2000) *Eur. J. Inorg. Chem.*, 2311–2326.
- Mahadevan, V., Gebbink, R. K. & Stack, T. D. (2000) *Curr. Opin. Chem. Biol.* **4**, 228–234.
- Que, L., Jr., & Tolman, W. B. (2002) *Angew. Chem. Int. Ed.* **41**, 1114–1137.
- Aboelella, N., Lewis, E. A., Reynolds, A. M., Brennesse, W. W., Cramer, C. J. & Tolman, W. B. (2002) *J. Am. Chem. Soc.* **124**, 10660–10661.
- Sawyer, D. T. (1991) *Oxygen Chemistry* (Oxford Univ. Press, New York).
- Pate, J. E., Cruse, R. W., Karlin, K. D. & Solomon, E. I. (1987) *J. Am. Chem. Soc.* **109**, 2624–2630.
- Baldwin, M. J., Ross, P. K., Pate, J. E., Tyecklar, Z., Karlin, K. D. & Solomon, E. I. (1991) *J. Am. Chem. Soc.* **113**, 8671–8679.
- Baldwin, M. J., Root, D. E., Pate, J. E., Fujisawa, K., Kitajima, N. & Solomon, E. I. (1992) *J. Am. Chem. Soc.* **114**, 10421–10431.